Characterization and Electrical Properties of Methyl-2-hydroxyethyl Cellulose Doped with Erbium Nitrate Salt

F. H. Abd-El Kader,[1] G. Said,[2] M. M. El-Naggar,[2] B. A. Anees[2]

[1]*Physics Department, Faculty of Science, Cairo University, Giza, Egypt*
[2]*Physics Department, Faculty of Science, Fayoum University, Fayoum, Egypt*

Received 27 November 2005; accepted 23 March 2006
DOI 10.1002/app.24482
Published online in Wiley InterScience (www.interscience.wiley.com).

ABSTRACT: X-ray diffraction, infrared (IR), and electrical properties for pure and Er $(NO_3)_3$-doped methyl-2-hydroxyethyl cellulose (MHEC) with concentrations of 0.5, 1, 2, 5, 7, and 10 wt % were studied. X-ray analysis indicates that the addition of Er $(NO_3)_3$, which is a crystalline material, to MHEC at concentrations 10 and 13 wt % leads to the formation of crystalline phases in the amorphous polymeric matrix. The appearance of the bending mode ν_2 and the combination mode $(\nu_1 + \nu_4)$ of Er $(NO_3)_3$ in the IR spectra of composite samples indicates the coordination of nitro group in the chains of MHEC. From the *I–V* characteristics, it was found that the charge transport mechanism in MHEC appears to be essentially space charge limited conduction, while the predominant mechanism in the composite samples is Poole–Frenkel. Values of both drift mobility (μ) and the charge carrier density (n) has been reported. The temperature dependence conductivity data has been analyzed in terms of the Arrhenius and Mott's variable range hopping models. Different Mott's parameters such as the density of states, $N(E_F)$, hopping distance (R), and average hopping energy (W) have been evaluated. J Appl Polym Sci 102: 2352–2361, 2006

Key words: IR spectroscopy; methyl-2-hydroxyethyl cellulose; rare earth metal salt; transient currents; electrical conductivity

INTRODUCTION

The wide usage of polymeric products in various fields of technology makes it necessary to investigate their structure, properties, and changes that take place under the addition of rare earth metal salts.

The current–voltage characterization, the DC electrical conductivity, and temporal variation of conduction current provide an understanding of the mechanisms of charge carrier transport, molecular motion, mobility of submolecules, and physical and chemical structures.[1] Valuable results can be revealed from the measurements of the temperature dependence of electric conductivity, because single molecules or molecular segments can either overcome a potential barrier as a consequent of continuous energy increase or chain decomposition.[2]

Methyl-2-hydroxyethyl cellulose (MHEC) is used in food, in cosmetics, and in aqueous-based paint systems. It has found applications as special chemicals in areas such as mineral and ceramic processing and polymerization.[3] MHEC is used in the optimization approach to the design of frost-resistance concrete.[4,5] For these purposes, it is desirable to improve a comprehensive characterization of MHEC when doped with different concentration of Er $(NO_3)_3$. In addition, the electrical properties of pure and Er $(NO_3)_3$-doped MHEC films have been studied in the temperature range 30–180°C. Conduction mechanisms have been identified with base of current–voltage and current–temperature measurements together with transient currents.

EXPERIMENTAL DETAILS

Methyl-2-hydroxyethyl cellulose (MHEC) was supplied by Sigma-Aldrich Company, USA. Its viscosity is ~15,000–20,000 cp. Erbium tri nitrate hydrated Er $(NO_3)_3 \cdot 6H_2O$ was supplied by Strem Chemicals Company, USA, with purity 99.9%. Weighted amounts of MHEC were dissolved in tri distilled water. Also weighted amounts of Er $(NO_3)_3$ were dissolved in very small amount of pure nitric acid at room temperature. Solutions of MHEC and Er $(NO_3)_3$ were mixed together with different weight percentages [0.5–10 wt % Er $(NO_3)_3$], using a magnetic stirrer, at 30°C. Films of appropriate thickness (~120 μm) were cast onto glass Petri dish of 10 cm diameter, and then dried in an oven at about 70°C for about 3 days until solvent was completely evaporated. Films were cut into square pieces having 1 cm side to fit the cell of measuring techniques.

Correspondence to: F. H. Abd-El Kader (Badawi.ali@gmail.com).

The infrared (IR) spectra analyses were performed using a PYE Unicam spectrophotometer over the range 500–4000 cm^{-1}, while X-ray diffraction patterns were obtained using XRD Scintag, USA, by CuK_α radaition. Transient and steady-state current–voltage characteristics were studied in the temperature range from 30–120°C and voltage range from 10 to 600 V. The current was measured by the means of an electrometer (Keithely 6517A) which was carefully shielded and grounded to avoid any extraneous electrical noise.

RESULTS AND DISCUSSIONS

Characterization

X-ray diffraction

Figure 1 shows the X-ray diffraction pattern of pure materials [Er $(NO_3)_3$ and MHEC] and their composites containing 1, 5, 10, and 13 wt % $Er(NO_3)_3$ at room temperature in the scanning range $6^\circ \leqslant 2\theta \leqslant 70^\circ$. Spectrum (a) of Er $(NO_3)_3$ in powder form shows different sharp reflection peaks which are characteristics of crystalline materials.[6] However spectrum (b) of MHEC cast film shows a broad so-called amorphous halo with a scattered intensity maximum corresponding to $2\theta = 22^\circ$. It reflects the absence of any diffraction lines indicating its amorphous nature.[7,8]

XRD patterns (c and d) of composite samples with concentrations 1 and 5 wt % Er $(NO_3)_3$ show an intense halo amorphous at peak position identical to that found in pure MHEC, but with less intensity. However, XRD pattern (e) of composite sample containing 10 wt % Er $(NO_3)_3$ is characterized by small five distinct crystalline peaks appearing at $2\theta = 15^\circ$, 30°, 33°, 42°, and 48° besides the amorphous one indicating the presence of Er $(NO_3)_3$ crystallites within the MHEC matrix. At relatively higher concentration of 13 wt % Er $(NO_3)_3$ composite sample, spectrum (f), additional two crystalline peaks appeared at $2\theta = 21^\circ$ and 31° while the amorphous halo peak disappeared completely. Also, the height of the pervious five crystalline peaks increased with increasing Er $(NO_3)_3$ content indicating the existence of relatively more crystallinity for 13 wt % Er $(NO_3)_3$ composite sample. This local ordering might have been accomplished by intramolecular and intermolecular interactions in the polymer structure. Thus, it can be thought that the crystallizing component could strongly modify the noncrystallizing behavior of the amorphous component in the amorphous/crystalline composites. For such composite samples, it can be suggested that the crystal form of Er $(NO_3)_3$ does not prevent the miscibility between MHEC and Er $(NO_3)_3$ and a complex between erbium tri nitrate with the polymer backbone being formed.

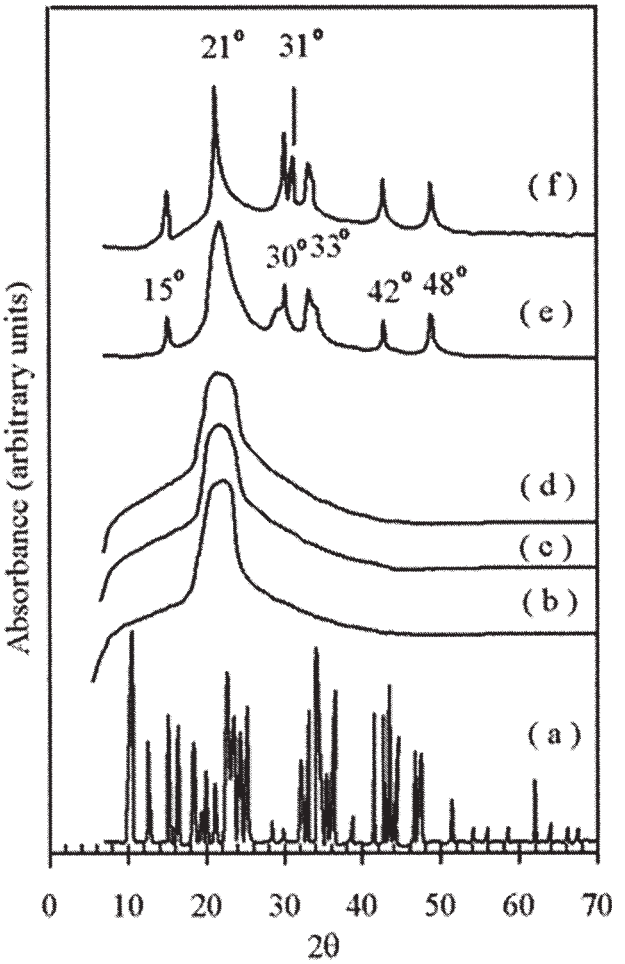

Figure 1 X-ray diffraction of (a) Er $(NO_3)_3$, (b) MHEC, (c) 1 wt %, (d) 5 wt %, (e) 10 wt %, and (f) 13 wt % Er $(NO_3)_3$-doped MHEC.

Infrared spectroscopy

Figure 2 shows the IR spectrum for pure [$Er(NO_3)_3$ and MHEC] and their composites containing 2 and 10 wt % $Er(NO_3)_3$ in the range of 500–4000 cm^{-1}. Spectrum (a) of Er $(NO_3)_3$ contains the symmetric N—O stretching frequency ν_1, the bending mode ν_2, the asymmetric stretching mode ν_3, the asymmetric in-phase bending mode ν_4, the first overtones $2\nu_1$, $2\nu_2$, and $2\nu_3$ and the combination modes $(\nu_1 + \nu_4)$ and $(\nu_1 + \nu_3)$. In addition, the broad band centered at 3700 cm^{-1} corresponding to ν(OH) which is probably due to H_2O present in the sample. These results are in agreement with that previously reported for trivalent metal nitrates.[9,10] The IR spectrum and assignment of the most evident absorption bands for MHEC is shown in pattern (b). The multiplicity and broadness of ν(OH) band observed in the 3000–3600 cm^{-1}region indicates the polymeric association of free hydroxyl groups and numerous of hydrogen-bonded (O—H) stretching vibration.[11,12] These two distinct absorption bands occurring at 2940 and 2900 cm^{-1} result from antisymmetric $\nu_{as}(CH_2)$ and

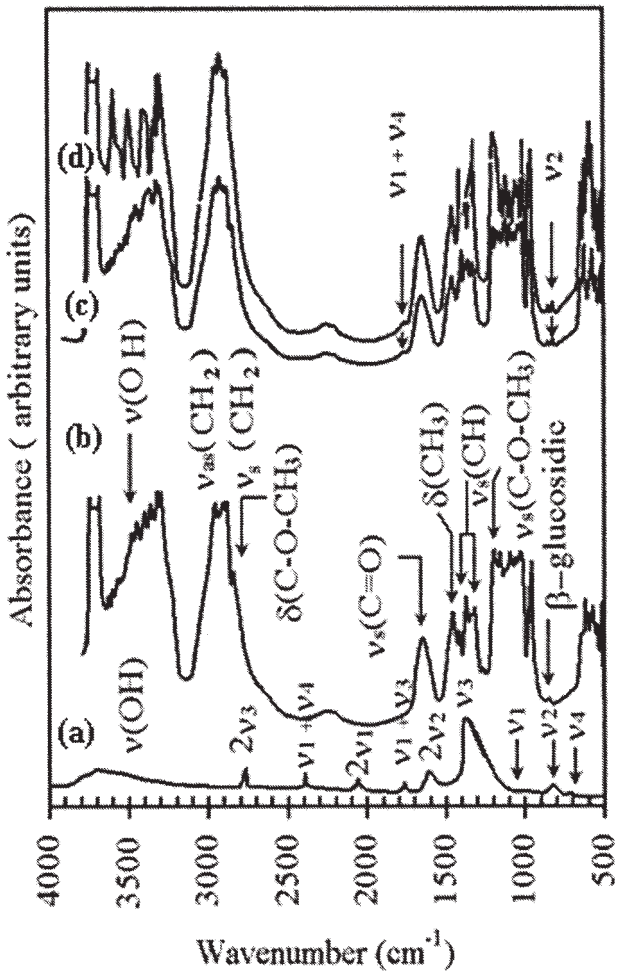

Figure 2 IR spectrum of (a) Er $(NO_3)_3$, (b) MHEC, (c) 2 wt %, and (d) 10 wt % $Er(NO_3)_3$-doped MHEC.

symmetric $\nu_s(CH_2)$ stretching bands of CH_2 groups, respectively. The band existing at 2839 cm^{-1} is due to (C—O—CH_3) deformation. Following these, there is no significant absorption band until about 1645 cm^{-1}, where a moderate band due to C=O stretching mode appears. This band can be attributed to the opening of the terminal ring in MHEC chains, giving a branched form.[13] The band existing at 1414 cm^{-1} is probably due to CH_3 deformation. The two bands appearing at 1372 and 1316 $cm^{-1}$are due to the bending mode $\nu_\delta(CH)$ of CH_2 groups. The absorption band appeared at 1191 cm^{-1} is related to symmetric ν_s(C—O—CH_3) stretching vibration. The small absorption band appeared at 850 cm^{-1} may be attributed to the C_1 group frequency (β-glucosidic linkage). These results are in agreement with that previously reported in literature[14,15] for cellulose derivatives.

The IR study is extended to examine doped MHEC samples with 2 and 10 wt % Er $(NO_3)_3$ patterns (c and d). In general, it appears from Figure 2 that there is no appreciable difference between the spectra of composite samples and pure MHEC except the changes in intensity and position of the absorption bands, appearance of new bands and overlapping. The peak position of the bands ν_s (C—O—CH_3) and ν_{as} (C—O) for 2 and 10 wt % Er $(NO_3)_3$ composite samples compared to pure MHEC is shifted by about (8 and 10 cm^{-1}) and (10 and 12 cm^{-1}) respectively, indicating that the oxygen atoms of C—O—CH_3 and C—O groups take part in the coordination.[16] It is worthy to note that two absorption bands at around 824 and 1760 cm^{-1} corresponding to the bending mode ν_2 and the combination mode (ν_1 + ν_4) respectively, are observed for both dopant concentrations. This may be taken as an indication to elucidate the formation of complexation, i.e., the coordination of nitrate group.

Electrical properties

Transient current

Current–time curves for pure MHEC and composite samples containing 0.5, 1, 2, 5, 7, and 10 wt % $Er(NO_3)_3$ at different temperatures (30 and 120°C) and fields (10 and 90 kV/m) were measured. Similar plots were obtained, and therefore the current–time

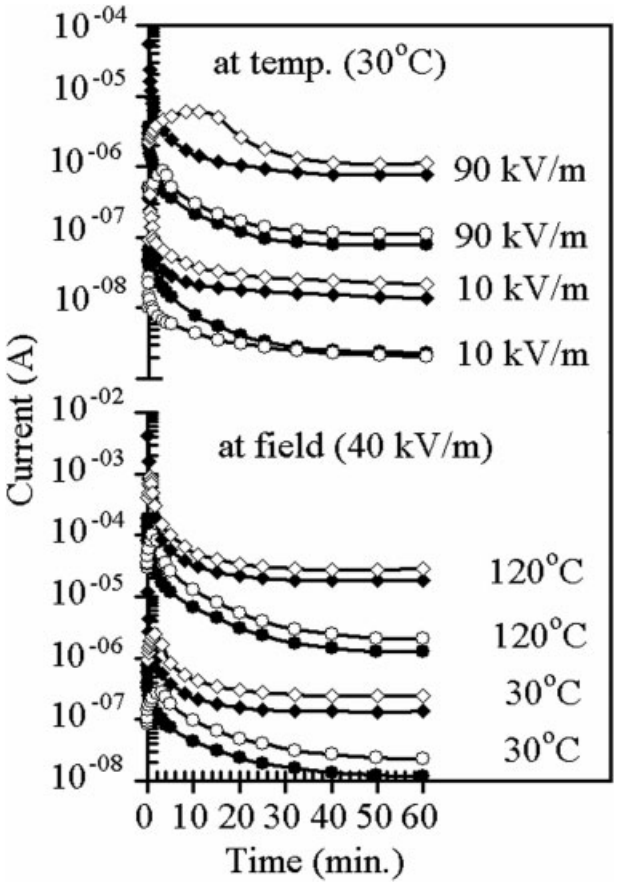

Figure 3 Transient current for both (●) MHEC and (◆) 2 wt % Er $(NO_3)_3$-doped MHEC at different temperatures and fields. Opened shapes refer to reverse polarity.

TABLE I
The Values of Mobility and Concentration of Charge Carriers for Pure and Er $(NO_3)_3$-Doped MHEC Samples at Different Temperatures and Constant Field 0.4 kV/cm

MHEC/Er$(NO_3)_3$ (wt/wt) %	μ(m^2 V^{-1} s^{-1})			n (m^{-3})		
	30°C	50°C	120°C	30°C	50°C	120°C
100/0.0	1.60×10^{-11}	2.40×10^{-11}	4.80×10^{-11}	9.30×10^{22}	1.04×10^{24}	1.10×10^{25}
99.5/0.5	1.92×10^{-11}	3.20×10^{-11}	5.70×10^{-11}	1.38×10^{23}	1.49×10^{24}	2.22×10^{25}
99/1	2.40×10^{-11}	3.70×10^{-11}	7.27×10^{-11}	2.20×10^{23}	2.88×10^{24}	2.91×10^{25}
98/2	3.20×10^{-11}	5.78×10^{-11}	9.60×10^{-11}	4.15×10^{23}	4.59×10^{24}	4.97×10^{25}
95/5	8.00×10^{-12}	9.60×10^{-12}	2.40×10^{-11}	2.10×10^{23}	4.42×10^{24}	3.62×10^{25}
93/7	8.73×10^{-12}	1.60×10^{-12}	2.18×10^{-11}	2.43×10^{23}	2.30×10^{24}	3.89×10^{25}
90/10	9.06×10^{-12}	1.14×10^{-11}	3.00×10^{-11}	1.75×10^{23}	3.25×10^{24}	2.65×10^{25}

curves for pure MHEC and 2 wt % Er $(NO_3)_3$ composite samples are taken as representatives (see Fig. 3). It is observed that the current response consists of two components; the first one decays very fast lasting few seconds and the second one decays with slow rate and attains steady state within 25–45 min from the application of the electric field. The initial curved part corresponds to the polarization of quickly reacting dipoles. For samples poled with higher fields and also at higher temperatures, the current tends to approach a steady value more rapidly. The field dominant behavior of these currents in composite samples shows that the initial currents are governed by the bulk phenomena such as polarization effect and/or interfacial phenomenon. The temporal decay of current may be due to trapping of charge carriers and reduction of electric field owing to the formation of Schottky layer in the vicinity of electrodes.[17] The case of tunneling as a possible mechanism can be discarded due to temperature dependence of transient behavior. However, the dipolar relaxation seems to be the major contributor to the transient current, as MHEC exhibits a polar character. The decline in the time dependence of transient current with increasing temperature may be attributed to the cumulative effect of rapid decrease of the relaxation time, a characteristic of transient phenomenon and the progressive increase of steady state conduction.

Application of direct and reverse polarities was carried out in succession. On reversing the polarity, the time t_{max} required for the conduction current to pass its maximum value decreases and the peak become narrower with the increase of temperature. On the contrary, the increase of field shows the effect of peak shift to longer times. The peaks observed in the reversed polarity curves can be envisaged by the arrival of a fraction of the ions at the electrode accumulating there as immobilized ions without discharging at the electrode.[18] These ions can become mobile again after the reverse of the polarity.

The order of magnitude of the drift mobility μ of charge carriers can be determined from the approximate relation[19,20]:

$$\tau = t_{max} = d^2/\mu V \tag{1}$$

where d is the thickness of the sample, V the applied voltage, and t_{max} the relaxation time corresponding to the peak current in I–T curve. Also the charge carrier density n can be calculated from the equation:

$$J = nq\mu E \tag{2}$$

where J is the current density at field strength E and q is the carrier charge. The calculated values of charge carrier concentrations and mobility for MHEC and the composite samples containing 0.5, 1, 2, 5, 7, and 10 wt % Er $(NO_3)_3$ at various temperatures and fields were calculated and are listed in Tables I and II. For all samples, the remarkable result is that the mobility increases significantly with increasing tem-

TABLE II
The Values of Mobility and Concentration of Charge Carriers for Pure and Er $(NO_3)_3$-Doped MHEC Samples at Different Fields and Constant Temperature (30°C)

MHEC/Er$(NO_3)_3$ (wt/wt) %	μ (m^2 V^{-1} s^{-1})			n (m^{-3})		
	0.1 (kV/cm)	0.4 (kV/cm)	0.9 (kV/cm)	0.1 (kV/cm)	0.4 (kV/cm)	0.9 (kV/cm)
100/0.0	8.00×10^{-10}	1.60×10^{-11}	1.20×10^{-11}	1.78×10^{20}	9.30×10^{22}	3.75×10^{23}
99.5/0.5	4.80×10^{-10}	1.92×10^{-11}	9.60×10^{-12}	7.75×10^{20}	1.38×10^{23}	6.63×10^{23}
99/1	3.69×10^{-10}	2.40×10^{-11}	6.86×10^{-12}	1.73×10^{21}	2.20×10^{23}	2.02×10^{24}
98/2	2.87×10^{-10}	3.20×10^{-11}	4.36×10^{-12}	7.39×10^{21}	4.15×10^{23}	7.29×10^{24}
95/5	3.00×10^{-10}	8.00×10^{-12}	4.80×10^{-12}	9.18×10^{20}	2.10×10^{23}	1.19×10^{24}
93/7	8.00×10^{-10}	8.73×10^{-12}	6.00×10^{-12}	2.65×10^{20}	2.43×10^{23}	7.96×10^{23}
90/10	2.40×10^{-10}	9.06×10^{-12}	6.15×10^{-12}	1.00×10^{21}	1.75×10^{23}	6.0×10^{23}

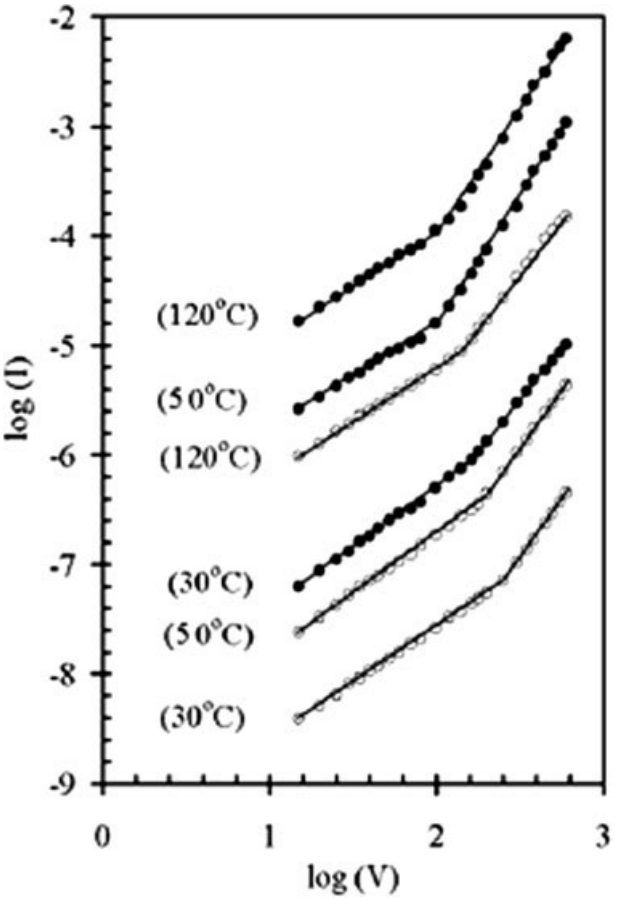

Figure 4 log(*I*)–log(*V*) for both (○) MHEC and (●) 2 wt % Er $(NO_3)_3$-doped MHEC at different temperatures.

perature, whereas a considerable decrease has been observed for increasing electric field. As the temperature increases, a reduction in the internal viscosity of the material allows the dipoles to rotate freely; hence the structural polarization takes place. The increase of drift mobility with temperature indicated that the conduction in the investigated samples is apparently due to thermally activated mobility. At higher electric fields, a change in mobility may occur faster than at lower field and also the recombination and/or scattering of charge carriers may be greater. Therefore, the decrease in drift mobility values may be considered as an indication of predominant ionic conduction.[21] The small values of mobility indicate the possibility of carriers transport by hopping mechanism. Besides, it can be deduced that the conduction enhancement with increasing both temperature and field is apparently due to the gradual increase of bulk generated free carriers density.

The effect of the addition of erbium tri nitrate into MHEC matrix up to 2 wt % is to reduce the barrier potential and increase the grain size, thereby causing grain boundary scattering to decrease and hence will increase the mobility.[22] At relatively higher dopant concentrations more than 2 wt % erbium tri nitrate, the mobility decreases monotonically. This may be attributed to the formation of molecular aggregates due to the inhomogeneous distribution of dopants.[23] If the dopants are not distributed homogenously to electron donor sites, this would cause partial polarization and formation of small conducting domains separated by some insulating regions of undoped polymer.[24]

Current–voltage characteristics

To investigate the conduction mechanism operating in the composite polymeric samples under investigation, the current–voltage characteristics at different temperatures are studied. The dependence of $\log I$ versus $\log V$ for pure and doped MHEC samples containing 0.5, 1, 2, 5, 7, and 10 wt % Er $(NO_3)_3$ shows the same behavior. Accordingly, Figure 4 shows $\log I$ versus $\log V$ plots at three different temperatures 30, 50, and 120°C for MHEC and 2 wt % Er $(NO_3)_3$-doped samples as representatives of whole series. Evidently, all plots indicate two different regions at various temperatures which depend upon

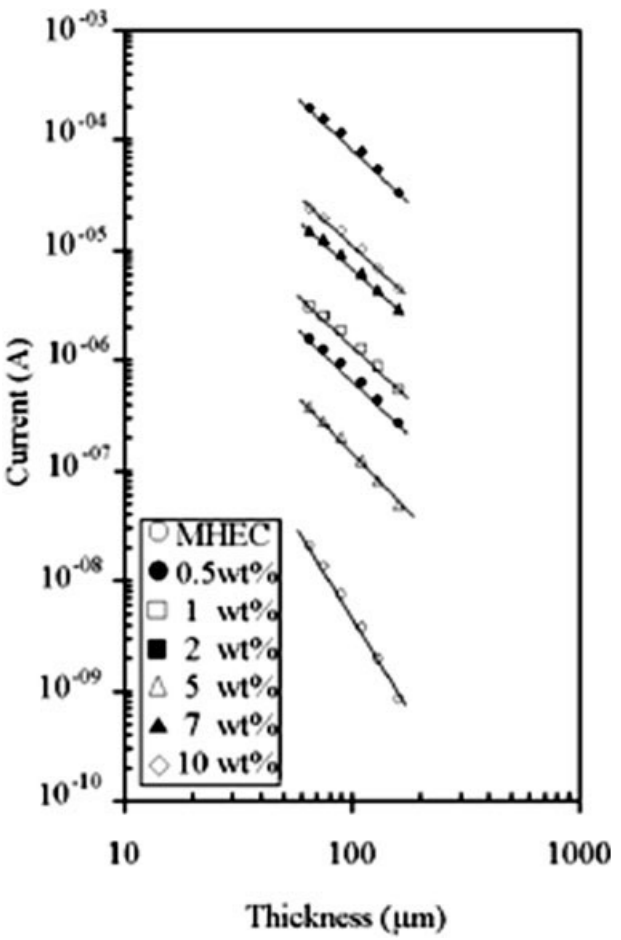

Figure 5 The current versus the thickness at temperature 50°C and applied voltage 200 V for pure and Er$(NO_3)_3$-doped MHEC.

TABLE III
The Values of Dielectric Constant for Pure and Er $(NO_3)_3$-Doped MHEC Samples at 10 kHz

MHEC/Er$(NO_3)_3$ (wt/wt) %	ε′ at 10 kHz		
	30°C	50°C	120°C
100/0	10.00	12.22	9.00
99.5/0.5	12.33	14.40	9.82
99/1	15.61	20.15	9.82
98/2	17.40	23.65	13.05
95/5	14.70	16.28	12.33
93/7	15.95	16.80	12.20
90/10	16.10	17.00	12.40

the applied field. In the low field region up to 1.3×10^6 V/m the slopes of the (I–V) relationship are found to be equal one, and hence Ohm's law is obeyed. In this first region, the conduction is governed by the resistances of the polymer material and controlled by thermally generated carriers. In the high field region, the slopes of (I–V) relationship are greater than one and the conduction becomes non-Ohmic.

Tunneling is not applicable in the present case as the thickness is pretty high (120 μm). Space charge effect may be present and contributing to the overall current.

Figure 5 shows I–V characteristics as a function of thickness at temperature 50°C in the non-Ohmic region for pure MHEC and 0.5, 1, 2, 5, 7, and 10 wt % Er $(NO_3)_3$-doped samples. The plots are straight lines with slope of (−3) for pure MHEC, while the slope is <−3 for the doped samples. So, we get $I \propto V^2$ and $1/d^3$ for pure MHEC, providing a supporting evidence for the existence of space charge conduction model.[25] According to this model space charge limited current density is given by:

$$J = \frac{9}{8}\mu_0\varepsilon_0\varepsilon'\theta\left(\frac{V^2}{d^3}\right) \tag{3}$$

where μ_0 is the free carrier mobility, ε_0 is the permittivity of free space, ε' is the dielectric constant, and θ is the ratio between the free electron (n_0) in the conduction band to the total density ($n_0 + n_t$), where n_t is the density of the trapped electrons. Experimentally θ is the ratio between the current densities at the beginning of the second region I_1 and at the end of the rise I_2, yields: $I_1/I_2 = \theta = n_0/(n_0 + n_t)$. The free carrier density in the conduction band n_0 and density of the trapped electrons n_t can be obtained using $n_0 = \varepsilon_0\varepsilon'\theta V_{tr}/qd^2$ and $n_t = 9\varepsilon_0\varepsilon' V_{tr}/8qd^2$ respectively, where V_{tr} is the voltage at which transition from Ohmic to square law region takes place. The values of ε' taken for all samples from dielectric measurement at a frequency 10 kHz. The calculated values of ε' are listed in Table III. By using the values of n_0 and n_t, the value of I_2 can be determined. From the value of I_2 the end of the rise up to trap-filled limited voltage V_{TFL} could be determined from Figure 4.

The free carrier mobility μ_0 can be now calculated from eq. (3), by using the experimental value of θ. It may be mentioned that when trap level exists, the electronic mobility is reduced by $1/\theta$,[26] and the effective electron drift mobility μ_e in an insulator with traps is therefore: $\mu_e = \mu_0\theta$. In the mean time, the trap concentration N_t is defined by $N_t = 2\varepsilon_0\varepsilon_r V_{TFL}/qd^2$ where V_{TFL} is the upper limit of the voltage at which sufficient charges have injected into the insulator to fill the traps.

The values of effective electron mobilities μ_e, the mobility of free charges μ_0, concentration of charge carries n_0, the density of trapped electrons n_t, and the trap concentration N_t for MHEC at different temperatures 30, 50, and 120°C are given in Table IV. The obtained values are quite comparable with those usually reported in literature for this class of polymeric materials.[27] It is clear from the Table IV that n_0, μ_0, and μ_e increase with increasing the temperature; on the contrary both n_t and N_t decrease with increasing temperature. The values of mobilities are found to be smaller than 10^{-4} m^2 V^{-1} s^{-1} indicating that polaron hopping between localized sites is involved in the process of carriers transport.

However, for all doped samples, it will be worthwhile to examine the fit of present results in close relation to electronic mainly Richardson–Schottky (RS) or Poole–Frenkel effects (PF) type conduction.

Several amorphous dielectric and semiconducting thin films exhibit at high electric field a current density of the following form[28,29]:

$$J \propto \exp(\beta E^{1/2}/kT) \tag{4}$$

where k is Boltzmann's constant, T is the absolute temperature, and β is the field lowering coefficient, whose theoretical for RS and PF values are given by: $\beta_{RS} = e[e/4\pi e_0 e']^{1/2}$ and $\beta_{PF} = 2e[e/4\pi e_0 e']^{1/2}$. From

TABLE IV
The Space Charge Parameters for MHEC

Temperature (°C)	n_0 (m^{-3})	n_t (m^{-3})	θ	μ_0 (m^2 V^{-1} s^{-1})	μ_e (m^2 V^{-1} s^{-1})	N_t (m^{-3})
30	2.00×10^{19}	13.00×10^{18}	0.60	6.32×10^{-10}	3.79×10^{-10}	2.85×10^{19}
50	4.00×10^{19}	8.00×10^{18}	0.83	4.65×10^{-8}	3.85×10^{-8}	2.00×10^{19}
120	6.25×10^{19}	5.90×10^{18}	0.91	3.15×10^{-7}	2.89×10^{-7}	1.19×10^{19}

TABLE V
The Theoretical and Experimental Values of β for Pure and Er $(NO_3)_3$-Doped MHEC Samples

MHEC/Er$(NO_3)_3$ (wt/wt) %	β_{exp} (10^{-5}) (eV $V^{-1/2}$ $m^{1/2}$)			β_{PF} (10^{-5}) (eV $V^{-1/2}$ $m^{1/2}$)		
	30°C	50°C	120°C	30°C	50°C	120°C
99.5/0.5	2.12	2.05	2.52	2.16	2.00	2.50
99/1	1.90	1.77	2.40	1.92	1.69	2.42
98/2	1.80	1.60	2.00	1.82	1.56	2.10
95/5	2.00	1.90	2.10	1.98	1.88	2.16
93/7	1.92	1.83	2.10	1.90	1.85	2.19
90/10	1.95	1.82	2.05	1.92	1.80	2.09

the slopes of log I versus $V^{1/2}$ (Figures not shown) for all composite samples at temperatures 30, 50, and 120°C, the experimental values of β_{exp} are calculated. Both experimental and theoretical values of β are listed in Table V. It can be seen that there is a close agreement between the experimental values of β and the theoretical value of β_{PF}. The small differences between the coefficients may result from the presence of donor and acceptor sites and/or the heterogeneity of the electrical field in the sample.[30]

A mere coincidence of β values may not be sufficient evidence for deciding the conduction mechanism.[31] Therefore, the actual conduction mechanism can be determined by studying the current–voltage characteristics of the composite sample 2 wt % erbium tri nitrate (as an example) at temperature 30°C using different top electrode materials, copper, nickel–chrome, and silver (see Fig. 6). It is clear that the effect of different electrode materials on the log (I) versus log ($V^{1/2}$) plots is found to be negligible within the experimental errors. Hence the Poole–Frenkel mechanism is the dominant conduction mechanism at all temperatures in the investigated composite samples. In addition, the linear variation of log σ versus $V^{1/2}$ as seen from Figure 7 for the composite sample 2 wt % erbium tri nitrate at temperatures 30, 50, and 120°C support this view point.

Electrical conductivity

Semi-logarithmic plots of DC electrical conductivity against the reciprocal of the absolute temperature for pure and Er $(NO_3)_3$-doped MHEC with concentrations of 0.5, 1, 2, 5, 7, and 10 wt % are shown in Figure 8. It can be seen that the general trend of the conductivity–temperature curves are similar; the curves passed through three main regions (I, II, and III). In low temperature region (I) below T_g, there is a rapid change in conductivity, while in high temperature region (III) there is a slight change in conductivity, the behavior in both regions for all samples was that of semiconductors. On the contrary, the intermediate region (II), the behavior was similar to that of metals, is apparently related to the diffused glass-transition temperature T_g of micro-Brownian motion of MHEC chains. T_g can usually be identified by the onset of the diffusional motion of large chain segments.

In general, the initial increase in conductivity with increasing temperature may be due to liberation of more charge carriers from traps and/or to the greater mobility through the amorphous region of polymer. However, the increase in conductivity at high temperatures may be accounted for the liberation of electrons or ions through the amorphous region of MHEC. In addition, the internal stresses in the doped samples may play a role in the motion of charge carriers. The fact that MHEC is considered as polar polymer may allow to quote also polarization conduction which becomes predominant at higher temperatures corresponding to region (III).

Erbium ions (E_r^{+3}) are coordinated through ionic bonds with the polar OR and CH_2OR [where R = (CH_2CH_2O) H or H or CH_3] groups belonging to the different chains in MHEC. This in turn reduces the intermolecular interaction between chains and expands the space between them. Therefore this

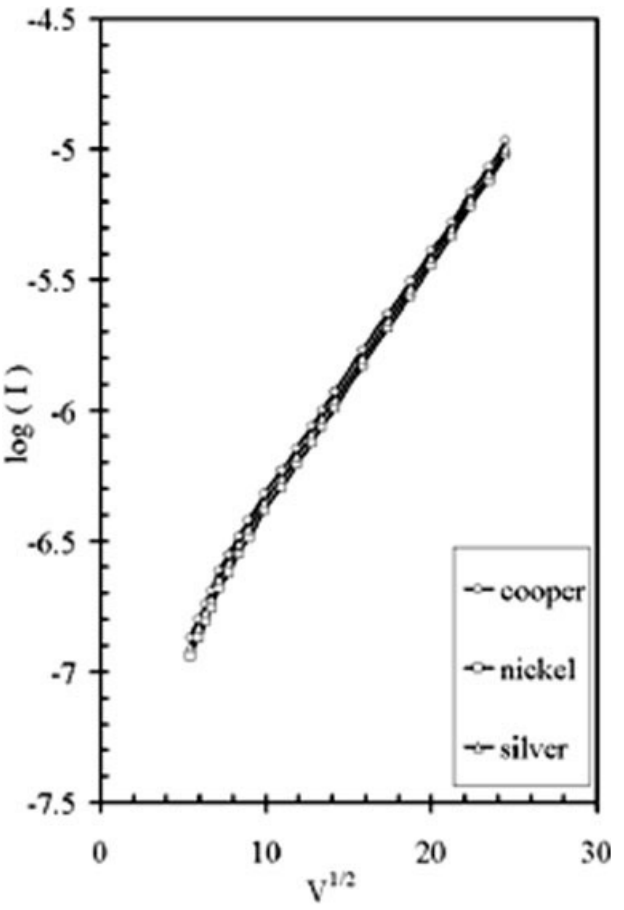

Figure 6 Electrode material effect on log(I) versus $V^{1/2}$ for 2 wt % Er $(NO_3)_3$-doped MHEC sample at 30°C.

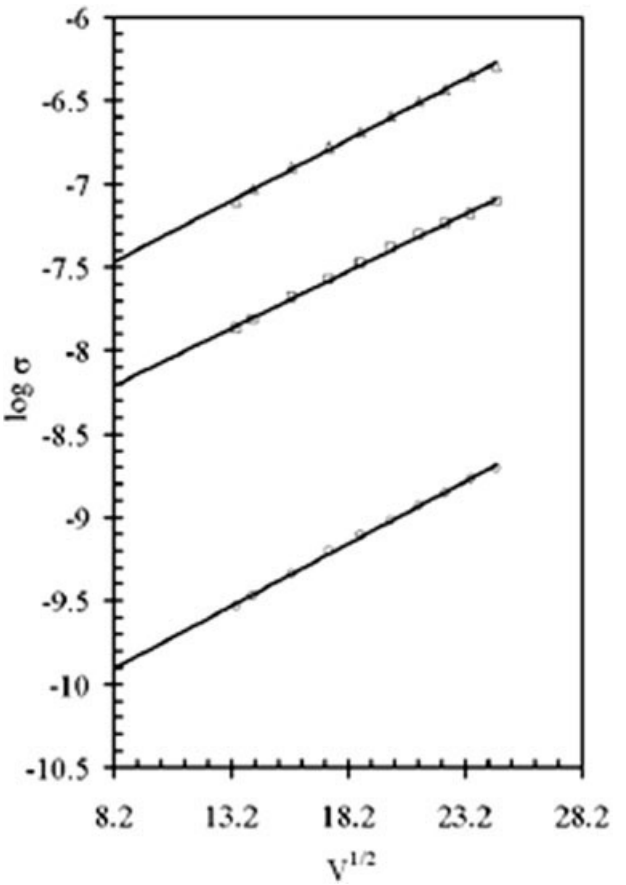

Figure 7 The variation of log(σ) versus $V^{1/2}$ for 2 wt % Er $(NO_3)_3$-doped MHEC sample at temperatures (○) 30°C, (□) 50°C, and (△) 120°C.

leads to an increase in the ionic mobility and reduction in the activation energy, which is in complete accordance with the results observed. It has been thought that the nonuniform doping causes heterogeneity, which leads to formation of nonstoichiometric charge-transfer complexes between the polymer and dopant.[23,32]

At low dopant concentrations from 0.5 to 2 wt % Er $(NO_3)_3$-doped samples, the conductivity increases monotonically with increasing dopant content over the temperature range from 30 to 180°C. This can be explained as being due to highly facilitated complex formation and the delocalization of more charge carriers transfer. It must also be noted that the dopant concentration 2 wt % Er$(NO_3)_3$ exhibits a maximum conductivity.

On the other hand, at relatively higher dopant concentrations more than 2 wt % Er $(NO_3)_3$ the conductivity decrease irregularly with increasing dopant content, giving values still higher than for MHEC. This may be attributed to the decrease in the mobility of charge carriers, mostly due to scattering of ionized molecular aggregates.

The temperature dependence of conductivity could be examined according to two basic existing theories, which are Arrhenius and Mott's variable range hopping (VRH) model. The log σ versus $1/T$ plots for the region (*I*) can not be represented by straight lines throughout the temperature interval applied and hence, the conductivity–temperature dependence does not obey an Arrhenius mechanism. This poor fit rules out of models of conduction in extended states of the valence band and next nearest neighbor hopping.[33] The results have been analyzed in the light of Mott's variable range hopping (VRH) model.[34]

A plausible mechanism is the VRH which according to Mott's formula obeys the relationship $\log(\sigma T^{1/2})$ is proportional to $T^{-1/4}$ in three dimensions (3D):

$$\sigma_{dc} = \frac{9e^2\nu_0}{64\alpha^2}\left(\frac{T_0}{T}\right)^{1/2} N(E_F)\ \exp\left[-\left(\frac{T_0}{T}\right)^{1/4}\right] \quad (5)$$

where $T_0 = 18.1\alpha^3/kN(E_F)$, ν_0 is the attempt frequency, $N(E_F)$ is the density of states at the Fermi energy and α describes the spatial extent of the localized wave function. Figure 9 shows that the conduc-

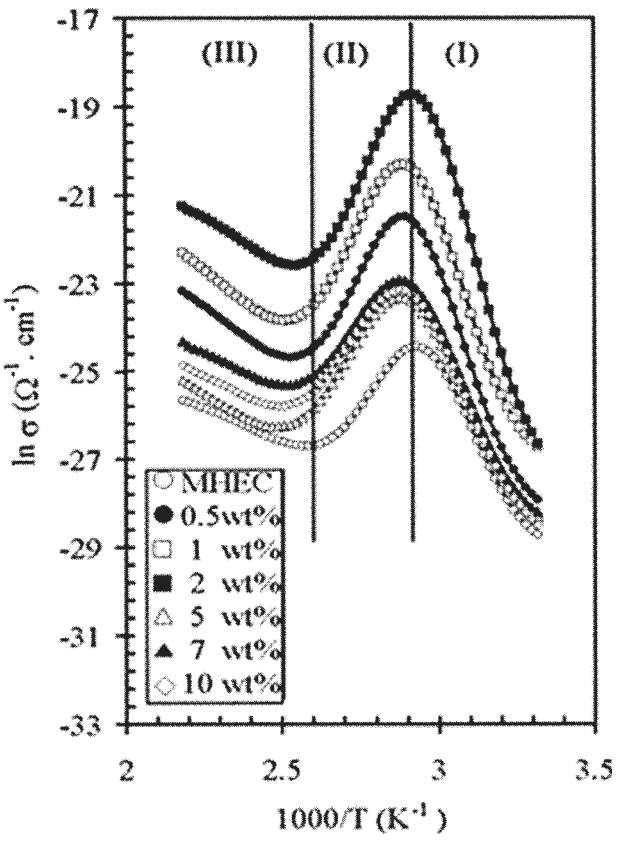

Figure 8 The variation of conductivity with the reciprocal of temperature for pure and Er $(NO_3)_3$-doped MHEC samples.

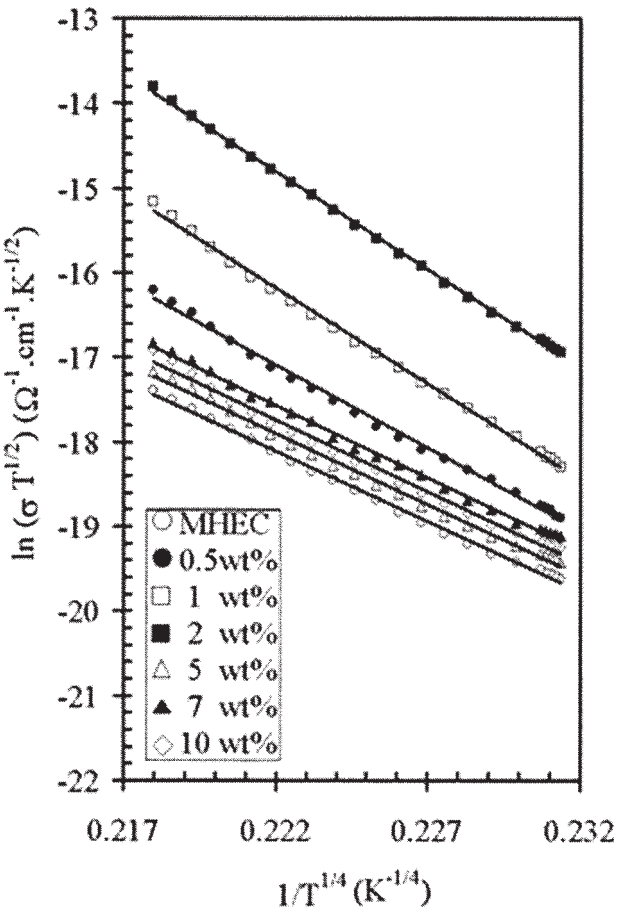

Figure 9 The relation between ln ($\sigma\ T^{1/2}$) and $1/T^{1/4}$ for pure and Er $(NO_3)_3$-doped MHEC samples.

tivity data as $\log(\sigma T^{1/2})$ versus $T^{-1/4}$ according to the 3D-VRH giving a good fit for all samples, independent of the doping level. The values of T_0, derived from the slope of the straight lines, are represented in Table VI. Assuming $\alpha^{-1} = 10^{-10}$ m for the amorphous materials,[35] $N(E_F)$ is calculated from T_0. In this conduction mechanism, there is a strong evidence for phonon-assisted hopping conduction for the samples under investigation. Such a behavior occurs in noncrystalline state in which the edges of the energy gaps are smoothed by tails of density of states. A mobility edge separates the localized from the nonlocalized levels, and a band at the Fermi level allows transition between the localized states inside the band or to levels above the mobility edge.

To check the validity of the Mott–Davis model for investigated samples, we made a rough calculation of some of Mott's parameters. The hopping distance (R) and the average hopping energy (W) can be determined by the following relations[36,37]:

$$R = \left[\frac{9}{8\pi\alpha kT\ N(E_F)}\right]^{1/4} \tag{6}$$

$$W = \left[\frac{3}{4\pi R^3 N(E_F)}\right] \tag{7}$$

The parameters of the conduction mechanism were determined by the above equations and are also given in Table VI. It is clear from the data in Table VI that the magnitude of the values of T_0, $N(E_F)$, and R are consistent with the values obtained for other amorphous polymers.[37] The realistic values of $N(E_F)$ and (W) indicate that Mott's VRH model is an appropriate mechanism of the conduction in region (I) for pure and Er $(NO_3)_3$-doped MHEC samples.

At higher temperatures (region III), the plots of $\log\sigma$ versus $1/T$ for all samples were linear as shown in Figure 8, confirming the validity of Arrhenius equation of the form: $\sigma = \sigma_0 \exp(-E_a/kT)$, where σ_0 is constant and E_a is the activation energy. Thus, the conductivity exhibits a thermally activated process, and the corresponding E_a values are in the range normally accounted for the kind of the conduction process in polysaccharides (see Table VI). At high temperatures, the hopping probability is dominated by the random spatial distribution of the atomic sites. The conductivity mechanism is mainly determined by hopping of carriers thermally activated into the band tails as monoenergetic trap states become thermodynamically accessible at higher temperatures. In fact, the variable range hopping regime dominating at lower temperature region (I) should change to the constant range regime with increasing temperature at region (III) because the hopping distance will reach

TABLE VI
The Variable Range Hopping Parameters and Arrhenius Activation Energy for Pure and Doped Er $(NO_3)_3$ MHEC Samples

MHEC/Er$(NO_3)_3$ (wt/wt) %	T_0 (K)	$N(E_F)$ (eV m^{-3})	R (nm)	W (eV)	E_a (eV)
100/0.0	9.40E + 8	2.17E + 29	0.16	0.30	0.92
99.5/0.5	6.00E + 8	3.40E + 29	0.14	0.26	0.85
99/1	3.00E + 8	6.81E + 29	0.12	0.22	0.73
98/2	1.00E + 8	2.04E + 29	0.09	0.17	0.65
95/5	2.00E + 8	1.02E + 29	0.10	0.20	0.74
93/7	2.5E + 8	8.17E + 29	0.11	0.21	0.81
90/10	3.00E + 8	6.81E + 29	0.12	0.22	0.85

its minimum value when the carriers jump between the nearest neighbor sites.[38]

CONCLUSIONS

1. On the basis of the data observed from IR spectroscopy and X-ray diffraction, it could be concluded that the formation of a complex between MHEC and Er $(NO_3)_3$ is possible within the investigated composition ranges.
2. From, X-ray diffraction it is noted that the addition of Er $(NO_3)_3$ above 5 wt % to MHEC changes the MHEC from the amorphous state to semi-crystalline state.
3. The realistic values of the density of states at Fermi energy and the low hopping energy indicate that the Mott's variable range hopping model is the appropriate mechanism of conduction and represented by $\ln(\sigma T^{1/2})$ versus $T^{-1/4}$ in the low temperature region for investigated samples. At higher temperature region the ln σ versus $1/T$ confirming the validity of Arrhenius relation and conductivity exhibits a thermally activated process.

References

1. Kar, T.; Choudhary, P. N. P. J Mater Sci Lett 2000, 19, 809.
2. Marianiava, D.; Lapcik, L.; Pisarcik, M. Acta Polym 1992, 34, 303.
3. Djuve, J.; Pugh, R. J.; Sjoblom, J. Colloids Surf A 2001, 186, 189.
4. Liedermann, K.; Lapcik, L., Jr. Carbohydr Polym 2000, 42, 374.
5. Klemm, A. J.; Marks, W. Building Environ 1999, 34, 369.
6. Tamboura, F. B.; Haba, P. M.; Gaye, M. Polyhedron 2004, 23, 1191.
7. Gedde, U. W. Polymer Physics; Chapman and Hall: London, 1995.
8. Wignall, G. D. In Physical Properties of Polymers, 2nd ed.; Mard, J. E., Ed.; American Chemical Society: Washington, DC, 1993.
9. Madan, S. K.; Chan, K. S. J Inorg Nucl Chem 1977, 39, 1007.
10. Taha, S.; Tosson, M. Thermochim Acta 1994, 236, 217.
11. Sakellariou, P.; Hassan, A.; Rowe, R. C. Polymer 1993, 34, 1240.
12. Tsukada, M.; Freddi, G.; Grighton, J. S. J Polym Phys 1994, 32, 243.
13. Mosichi, V.; Calvini, P.; Mattagno, G.; Righini, G. Cellul Chem Technol 1990, 24, 263.
14. Biswal, D. R.; Singh, R. P. Carbohydr Polym 2004, 57, 379.
15. Xiuyuan, N.; Yuefang, H.; Bailin, L.; Xi, X. Eur Polym J 2001, 37, 201.
16. Bezerra, R. F.; Melo, D. M. A.; Vicentini, G.; Zinner, K. B. J Alloys Compd 2002, 344, 120.
17. Sessler, G. M.; Hans, B.; Yoon, D. Y. J Appl Phys 1986, 60, 318.
18. Shehap, A.; Abd-Allah, R. A.; Basha, A. F.; Abd El-Kader, F. H. J Appl Polym Sci 1998, 68, 687.
19. Ispda, S.; Mjiaji, H.; Asai, K. Jpn J Appl Phys 1973, 12, 1799.
20. Jain, K.; Rastogi, A. C.; Chopra, K. L. Phys Status Solidi A 1973, 20, 167.
21. Jain, V. K.; Gupta, C. L.; Jain, N. K. Indian J Pure Appl Phys 1978, 16, 625.
22. Petritz, R. L. Phys Rev 1956, 104, 1508.
23. Reddy, N. V.; Rao, V. V. R. N. J Mater Sci Lett 1992, 11, 1036.
24. Nalwa, H. S. J Mater Sci 1992, 27, 210.
25. Leditzky, G.; Leising, T. J Phys D: Appl Phys 1994, 27, 2185.
26. Rose, A. Phys Rev 1955, 97, 1538.
27. Chutia, J.; Barura, K. J Phys D: Appl Phys 1980, 13, 9.
28. Qi, P.; Wang, J. F.; Su, W. B.; Chen, H. C.; Zang, G. Z.; Wang, C. M.; Ming, B. Q. Mater Sci Eng B 2005, 119, 94.
29. Gupta, R. K.; Singh, R. A. Mater Chem Phys 2004, 86, 279.
30. Rao, N. V. R. N.; Mohender, T.; Rao, B. S. J Non-Cryst Solids 1988, 104, 224.
31. Simmons, J. G. Phys Rev 1967, 155, 657.
32. Sharama, A. K.; Adinarayara, V.; Sagar, D. S. J Mater Sci 1991, 12, 247.
33. Zamora, F.; Ganzalez, M. C. Polymer 1997, 38, 263.
34. Mott, N. F. Adv Phys 1972, 21, 785.
35. Singh, R.; Kaur, A.; Yadav, K. L.; Bhattacharya, B. Curr Appl Phys 2003, 3, 235.
36. Okutan, M.; Bakan, H. I.; Karkmaz, K.; Yakuphanoglu, F. Phys B 2005, 355, 176.
37. Kumar, N.; Vadera, S. R.; Jana, P. C. Polymer 1992, 33, 242.
38. Mott, N. F.; Davis, E. A. Electronic Processes in Non-Crystalline Materials, 2nd ed.; Clarendon Press: Oxford, 1979.